

Diagnosis of a New Neutral Gauge Boson at the LHC and ILC for Snowmass 2013

Tao Han^a, Paul Langacker^{b,c}, Zhen Liu^a and Lian-Tao Wang^d

^a*Pittsburgh Particle physics, Astrophysics, and Cosmology Center,
Department of Physics and Astronomy, University of Pittsburgh,
3941 O'Hara St., Pittsburgh, PA 15260, USA*

^b*School of Natural Science, Institute for Advanced Study,
Einstein Drive, Princeton, NJ 08540, USA*

^c*Department of Physics, Princeton University,
Princeton, NJ 08544, USA*

^d*Department of Physics, Enrico Fermi Institute,
and Kavli Institute for Cosmological Physics,
University of Chicago, Chicago, IL 60637-1434, USA*

ABSTRACT: A $U(1)'$ or Z' is generic in many scenarios of physics beyond the Standard Model, such as string theory compactifications, GUTs, extra-dimensions, compositeness, dynamical electroweak symmetry breaking, dark-sector models, etc. We study the potential of probing a TeV-scale Z' with electroweak couplings in future experiments. In particular, we focus on two scenarios: (1) If a Z' is discovered at the LHC, what is the potential of measuring its mass and width and to distinguish between benchmark models utilizing various observables, especially asymmetries, at a high luminosity LHC and the ILC. (2) If the Z' is not accessible as a clear resonance signal, what is the exclusion reach at the ILC.

KEYWORDS: Z' , LHC, ILC

Contents

1	Z' Parameters	2
2	Case 1: Z' Observable at the LHC	4
2.1	LHC Searches	4
2.1.1	Leptonic Final States	5
2.1.2	Hadronic Final States	7
2.2	ILC Effects	9
3	Case 2: Z' Beyond the LHC Reach	11
4	Conclusions	12
A	Z' at the LHC	13
A.1	Narrow Width Approximation	15
A.2	Angular Distribution	16
A.3	Final State Polarization	17
A.4	Beyond the Narrow Width Approximation	17
A.5	Finite Mass Corrections	18
B	Z' at the ILC	18
B.1	No Polarization	18
B.2	Fixed Initial State Polarization	19
B.3	Polarization Asymmetries	20

1 Z' Parameters

Additional colorless vector gauge bosons (Z') occur in many extensions of the Standard Model (SM), in part because it is generically harder to break additional abelian $U(1)'$ factors than non-abelian ones¹. The existence of a Z' could have many other possible implications, including an NMSSM-like solution to the μ problem (and the possibility of electroweak baryogenesis), new F and D term contributions to the lightest scalar mass, an additional Higgs singlet, additional neutralinos (with collider and dark matter consequences), new vector (under the SM) fermions for anomaly cancellation, and many possibilities for neutrino mass. Other possibilities involve interactions with dark matter, the mediation of supersymmetry breaking, FCNC (for family non-universal couplings), associated charged W' s, and the production of superpartners and exotics. The Z' couplings could also give clues about a possible embedding of the $U(1)'$ into a more fundamental underlying theory. Although Z' s can occur at any scale and with couplings ranging from extremely weak to strong, we concentrate here on TeV-scale masses with couplings not too different from electroweak, which might therefore be observable at the LHC or future colliders.

Following the notation in [1], we define the couplings of the SM and additional neutral gauge bosons to fermions by

$$-L_{NC} = eJ_{em}^\mu A_\mu + g_1 J_1^\mu Z_{1\mu}^0 + g_2 J_2^\mu Z_{2\mu}^0, \quad (1.1)$$

with

$$J_\alpha^\mu = \sum_i \bar{f}_i \gamma^\mu [\epsilon_L^{\alpha i} P_L + \epsilon_R^{\alpha i} P_R] f_i. \quad (1.2)$$

The SM (Z_1^0) parameters are $g_1 = g/\cos\theta_W$ and $\epsilon_L^{1i} = t_{3L}^i - \sin^2\theta_W q^i$, $\epsilon_R^{1i} = -\sin^2\theta_W q^i$, where q^i is the electric charge of f_i in units of $|e|$ and $t_{3L}^i = \pm 1/2$ is the third component of weak isospin. We will absorb g_α into the chiral charges² by defining

$$g_{L,R}^{1i} \equiv g_1 \epsilon_{L,R}^{1i}, \quad g_{L,R}^{2i} \equiv g_2 \epsilon_{L,R}^{2i}. \quad (1.3)$$

When it does not cause confusion we will drop the superscript 2 on $g_{L,R}^{2i}$. It will also be convenient to define the vector and axial couplings and the asymmetry parameters

$$g_{V,A}^i \equiv g_L^i \pm g_R^i, \quad A_i \equiv \frac{g_L^{i2} - g_R^{i2}}{g_L^{i2} + g_R^{i2}} = \frac{2g_V^i g_A^i}{g_V^{i2} + g_A^{i2}}, \quad (1.4)$$

for $i = u, d, e, \nu, \dots$. Analogous definitions hold for the $g_{L,R}^{1i}$.

Assuming negligible (ordinary and kinetic) $Z - Z'$ mixing [6, 10, 11]) and family universality, the relevant Z' parameters are $M_{Z'}$, $\Gamma_{Z'}$, and the chiral couplings $g_{L,R}^i$ for $i = u, d, e$, and ν . A lower bound on $\Gamma_{Z'}$ (the ‘‘minimal’’ width) can be calculated in terms of the

¹For reviews, see [1–4]. Specific properties are reviewed in [5–11].

²The gauge coupling g_2 is not really a separate parameter, because it can be absorbed in the chiral couplings, as in (1.3). However, the separate extraction of g_2 would become meaningful if the charges were established to correspond to an embedding in a nonabelian group of some other model with well-defined normalization, such as the E_6 and LR models.

other parameters from the decays into the SM fermions, but a larger $\Gamma_{Z'}$ is possible due to decays into Higgs particles, superpartners, right-handed neutrinos, exotic fermions (such as those needed in some Z' models for anomaly cancellation), or other Beyond the Standard Model (BSM) particles [12, 13]. We will usually assume as well that the $U(1)'$ charges commute³ with $SU(2)$, so that there are only five relevant chiral charges,

$$g_L^u = g_L^d \equiv g_L^q, \quad g_R^u, \quad g_R^d, \quad g_L^e = g_L^\nu \equiv g_L^\ell, \quad g_R^e. \quad (1.5)$$

Ideally, one would like to determine these, as well as $M_{Z'}$ and $\Gamma_{Z'}$, in a model-independent way from collider as well as existing and future precision data. In practice, the existing limits are sufficiently stringent that we may have to resort to considering specific benchmark models. For illustration, we will consider the well-known χ , ψ , and LR models, associated with the breakings $SO(10) \rightarrow SU(5) \times U(1)_\chi$, $E_6 \rightarrow SO(10) \times U(1)_\psi$, and $SU(2)_L \times SU(2)_R \times U(1)_{B-L} \rightarrow SU(2) \times U(1)_Y \times U(1)_{LR}$ (for $g_R = g$), respectively. We will also consider $Z_\eta = \sqrt{\frac{3}{8}}Z_\chi - \sqrt{\frac{5}{8}}Z_\psi$, associated with a certain compactification of the heterotic string, and the B-L model⁴ with charge $(B-L)/2$. The charges for these benchmark models are listed in Table 1. For the E_6 , LR, and B-L models we will take for the reference value of g_2 the GUT-normalized hypercharge coupling

$$g_2 = \sqrt{\frac{5}{3}} g \tan \theta_W \sim 0.46, \quad (1.6)$$

which is an approximation to the simplest E_6 prediction [14] for the GUT models and follows for $g_R = g$ in $SU(2)_L \times SU(2)_R \times U(1)_{B-L}$. We will also consider the sequential model with $g_2 = g_1$ and $\epsilon_{LR}^{2i} = \epsilon_{LR}^{1i}$.

	χ	ψ	η	LR	B-L	SSM	
D	$2\sqrt{10}$	$2\sqrt{6}$	$2\sqrt{15}$	$\sqrt{5/3}$	1	1	
$\hat{\epsilon}_L^q$	-1	1	-2	-0.109	1/6	$\hat{\epsilon}_L^u$	$\frac{1}{2} - \frac{2}{3}\sin^2\theta_W$
						$\hat{\epsilon}_L^d$	$-\frac{1}{2} + \frac{1}{3}\sin^2\theta_W$
$\hat{\epsilon}_R^u$	1	-1	2	0.656		$\hat{\epsilon}_R^u$	$-\frac{2}{3}\sin^2\theta_W$
$\hat{\epsilon}_R^d$	-3	-1	-1	-0.874		$\hat{\epsilon}_R^d$	$\frac{1}{3}\sin^2\theta_W$
$\hat{\epsilon}_L^\ell$	3	1	1	0.327	-1/2	$\hat{\epsilon}_L^\nu$	$\frac{1}{2}$
						$\hat{\epsilon}_L^e$	$-\frac{1}{2} + \sin^2\theta_W$
$\hat{\epsilon}_R^e$	1	-1	2	-0.438		$\hat{\epsilon}_R^e$	$\sin^2\theta_W$

Table 1. Benchmark models and couplings, with $\epsilon_{L,R}^i \equiv \hat{\epsilon}_{L,R}^i/D$.

³One exception is the benchmark sequential model, in which $g_{L,R}^{2i} = g_{L,R}^{1i}$. This could possibly emerge from a diagonal embedding of the SM in a larger group, or for Kaluza-Klein excitations in an extra-dimensional theory.

⁴The $B-L$ charge usually occurs in a linear combination with $T_{3R} = Y - \frac{B-L}{2}$, where $Y = Q - T_{3L}$, as in the χ and LR models. Here we consider a simple $B-L$ charge as an example of a purely vector coupling.

2 Case 1: Z' Observable at the LHC

Typical Z' models with electroweak couplings should be observable⁵ at the LHC as resonances in the dilepton channels for masses up to $\sim 4\text{--}5$ TeV for $\sqrt{s} = 14$ TeV and an integrated luminosity of 100 fb^{-1} . There have been extensive studies of diagnostic possibilities⁶ of the Z' couplings at the LHC utilizing the cross sections

$$\sigma^f \equiv \sigma[f\bar{f}] \equiv \sigma_{pp \rightarrow Z' \rightarrow f\bar{f}} = \sigma_{Z'} B(Z' \rightarrow f\bar{f}) \quad (2.1)$$

for decays into the final state $f\bar{f}$ for $f = \ell, \tau, t, b$ (with $\ell = e, \mu$), as well as forward-backward or charge asymmetries, rapidity distributions, and possible final state polarizations for $\tau^-\tau^+$ or $t\bar{t}$. Other possible probes include $\Gamma_{Z'}$ from the lineshape, and various rare decay modes and associated productions. It was generally concluded that significant diagnostic probes of the couplings would be possible for Z' masses up to around 2.5 TeV.

However, ATLAS [35] and CMS [36] have already excluded dilepton resonances corresponding to standard benchmark Z' s below $\sim 2.5\text{--}2.9$ TeV, so even if a Z' is observed in future LHC running it will be difficult to carry out detailed diagnostics. We have therefore re-examined what might be learned for a relatively heavy Z' , allowing for high integrated luminosities of 300 and 3000 fb^{-1} at the LHC, in combination with observations at the ILC with $\sqrt{s} = 500$ GeV and integrated luminosity of 500 fb^{-1} , or at 1 TeV with 1000 fb^{-1} , for fixed e^\mp polarizations. We also consider the possibility of additional ILC running with reversed polarizations. We consider two illustrative cases: (1) a 3 TeV Z' observed directly at the LHC and indirectly at the ILC; (2) a more massive Z' observed only by indirect effects at the ILC. Future studies will also include indirect constraints from existing and future precision experiments.

2.1 LHC Searches

The formalism relevant to the production and decay of a Z' at the LHC is summarized in Appendix A. We assume in this section that a narrow colorless resonance has been observed as a peak in the $\ell^-\ell^+$ distribution at the LHC at mass $M_{Z'}$, and that the lepton angular distribution has identified that the resonance has spin-1 [20, 25]. Assuming family universal couplings and neglecting $Z - Z'$ mixing (known to be small from precision electroweak studies [6, 10, 11]), there remain to be determined the five chiral couplings in (1.5) as well as $\Gamma_{Z'}$. Ideally, one would like to determine these in as model-independent a way as possible.

The simplest observables (other than $M_{Z'}$) are the cross sections $\sigma^f = \sigma_{Z'} B(Z' \rightarrow f\bar{f})$ after subtracting backgrounds, especially for $f = e, \mu$. However, the cross sections have uncertainties from the parton distribution functions (PDFs), higher-order terms, and the luminosity. Furthermore, they are inversely proportional to $\Gamma_{Z'}$, as in (A.14), so they do not allow a determination of the absolute couplings, even in principle. Also, the leptonic rates depend only on a linear combination of the u and d couplings (roughly 2 to 1 at

⁵The reach is reduced if the dilepton branching ratios are significantly reduced due to BSM decay channels [12, 13].

⁶See, for example, [12, 13, 15–34]. Other studies are reviewed in [1, 4, 8].

the LHC), unless there is significant information from the rapidity distribution (which is unlikely at the LHC).

The $\Gamma_{Z'}$ ambiguity can be eliminated and the PDF/higher order uncertainties can be reduced by considering ratios of observables. If one can tag the $f = b$ and t final states well enough⁷ then the ratios of the rates for $f = \ell, b, t$ could in principle determine the ratios of $g_L^{q^2} + g_R^{u^2}, g_L^{q^2} + g_R^{d^2}$, and $g_L^{\ell^2} + g_R^{e^2}$ (again assuming family universality). These could be promoted to absolute measurements if $\Gamma_{Z'}$ can be extracted from the lineshape, since the product $\sigma^f \Gamma_{Z'} = \sigma_{Z'} \Gamma(Z' \rightarrow f\bar{f})$ depends only on the absolute couplings.

Forward-backward or charge asymmetries could yield additional information. From (A.20) we see that $g_R^{f^2}/g_L^{f^2}$ can be determined for $f = \ell, u, d$ if charge identification is available for ℓ, t, b , respectively. This is again independent of $\Gamma_{Z'}$ and involves reduced PDF uncertainties. Final state polarization effects for $f = \tau$ or t could carry complementary information, which could increase the accuracies of the determinations and/or help to test our assumption of family universality. Off-pole interference with standard model (mainly γ and Z) backgrounds could also in principle yield information such as the signs of the couplings [30, 33].

As stated previously, however, the existing LHC limits are sufficiently strong that it will most likely not be possible to obtain significant model-independent determinations of the couplings from the LHC alone. Nevertheless, some of the observables could at least allow discrimination between the benchmark models.

2.1.1 Leptonic Final States

The leptonic final states are very clean at the LHC. The standard model dilepton background is at the attobarn level, negligible compared to the femtobarn-level signal. We tabulate the cross sections and total widths for our benchmark models in Table 2 for $M_{Z'} = 3$ TeV. These widths are “minimal”; if the Z' can decay into final states other than standard model fermions, the total width will increase, resulting in a suppression of the standard model fermion branching fractions as well as the appearance of new visible (invisible) final states like $W_R^+ W_R^-$ (sterile $\nu_R^c \nu_R$).

	χ	ψ	η	LR	B-L	SSM
width (3 TeV Z') (GeV)	34.7	15.7	18.9	61.4	27.4	88.7
σ^e (fb)	0.850	0.430	0.503	1.006	1.004	1.602

Table 2. The minimal widths for the benchmark Z' models and the cross sections $\sigma^e = \sigma[e^-e^+] = \sigma_{Z'} B(Z' \rightarrow e^-e^+)$ at the (14 TeV) LHC for dielectron final states in the mass window 2.8–3.2 TeV. The acceptance of the electron-positron pair is taken to be 78%.

We simulate the signal and background events using MadGraph5 [37] with input model files generated by FeynRules [38], using proton parton distribution functions (PDF) set CTEQ6l1 [39]. The generated events then pass through Pythia6 [40] to perform parton showers and then Delphes [41] for detector simulation using the Snowmass Delphes3 card.

⁷The total dijet rate may be impossible to observe for a Z' with electroweak coupling.

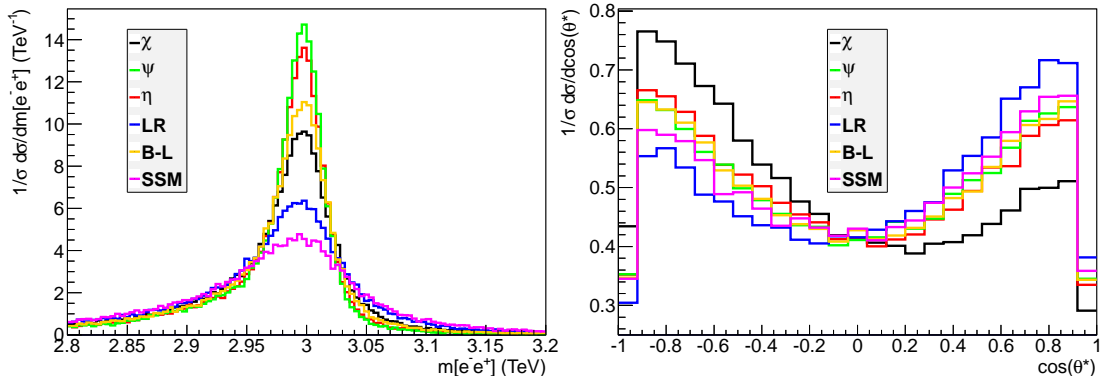


Figure 1. *Left panel:* the invariant mass distribution of the dielectron system for the benchmark models for a 3 TeV Z' at the LHC at 14 TeV; *Right panel:* the angular distribution of the electrons in the CM frame with respect to the rapidity (boost) direction of the system in the lab frame, integrated over the dielectron rapidity y .

We show the invariant mass distributions and the angular distributions in the center of mass (CM) frame of the dielectron system for these benchmark models in Figure 1. One can extract the mass, width, and total rate σ^e from the invariant mass distribution as shown in the left panel⁸. The dimuon final state is similar. The energy resolution for high energy muons is worse than for electrons according to the Snowmass detector simulation. As a result, dimuon final states will provide additional statistics for Z' discovery but won't contribute much to the mass and width determinations.

The forward-backward asymmetry A_{FB} , defined in (A.20) (which is equivalent to the charge asymmetry A_c in (A.21)), can be obtained directly by counting, from the charge asymmetry, or by fitting to the angular distribution shown in the right panel of Figure 1 for the benchmark models. From (A.20) one sees that A_{FB} is sensitive to the difference between the left and right- chiral couplings-squared of the leptons and of the quarks. Of course, there is no forward-backward asymmetry in a pp collider at zero Z' rapidity y , but there can be an asymmetry for nonzero y . We define the forward direction with respect to the rapidity (boost) direction of the Z' or equivalently of the dielectron system. The (mainly valence) quark direction is usually the same as the boost direction at the LHC. However, around 20% of the events have the anti-quark direction along the boost direction (the contamination factor). This contamination factor varies for different PDF sets, adding additional theoretical uncertainties. It also varies somewhat with the Z' model because of the different relative couplings of up-type and down-type quarks.

In order to estimate the sensitivity to the Z' parameters, we have simulated the line-shape and angular distributions for each of our benchmark models, assuming the minimal width, and then “fit” to the simulated data to determine the uncertainties in the extracted

⁸The rapidity distribution of the dielectron pair could in principle be useful for separating the effects of the u and d . In practice, however, there is little sensitivity for $M_{Z'} \gtrsim 3$ TeV.

parameters. We show the fitting results for the masses and widths of the Z' in the left panel of Figure 2, and the simulated cross section and forward-backward asymmetries in the right panel. The two contours are for the LHC at 14 TeV and 300 fb^{-1} (blue) and 3000 fb^{-1} (red). The fitting for the mass and width is model-independent. We fit the invariant mass distribution by a Breit-Wigner resonance convoluted with a Gaussian distribution for the smearing from the electron energy resolution. We assume 0.7% systematic uncertainties for the mass and width ($\sqrt{2}$ times the electron energy resolution 0.5%). We see that $M_{Z'}$ can be reproduced to around 10 GeV, i.e., better than one percent. $\Gamma_{Z'}$ can also be determined to around 10 GeV, but from Table 2 and Figure 2 this is very crude (e.g., 30-60%) for the minimal widths in most of the benchmark models. The total width and mass precision is dominated by systematic uncertainties: one can see that the improvement from 300 fb^{-1} to 3000 fb^{-1} is not significant. Nevertheless, the LHC is the only planned facility that can measure these quantities to any precision⁹.

We also show the forward-backward asymmetry and cross section determinations¹⁰. In addition to the statistical uncertainties, we take the systematic uncertainties $10\% \oplus 2\%$ ($6\% \oplus 2\%$) for the cross section for the LHC at 300 fb^{-1} (3000 fb^{-1}). The 10% (6%) are the correlated uncertainties (e.g., PDF and luminosity uncertainties) that will cancel when taking the ratios of cross sections, leaving 2% systematics for the forward-backward asymmetry. A_{FB} can be determined very well for asymmetric models such as the Z_χ and Z_{LR} , approximately 20% (5%) at the LHC 14 TeV with 300 fb^{-1} (3000 fb^{-1}). The absolute error is comparable for the other (more symmetric) models. The contours in Figure 2 indicate that there is some reasonable possibility of distinguishing some of the benchmark models with minimal width at the LHC 14 TeV. However, there is not much possibility for model-independent studies based on the dielectron observables alone.

2.1.2 Hadronic Final States

The hadronic final states of the 3 TeV Z' are particularly important. Once combined with the leptonic channels, under the assumption of family universality, one can in principle obtain the absolute values of the Z' coupling strength to both leptons and hadrons. On the other hand, one faces the difficulties of huge QCD backgrounds. In this section we discuss the possibility of observing these channels at the LHC.

We list the parton level cross section for both signal and irreducible background at the LHC 14 TeV in Table 3. The cross sections for these models for the dijet final state, including up, down, charm and strange quarks, are at the femtobarn level. The QCD background, after preliminary cuts, is ~ 1000 times larger than the signal. More strict cuts and selection criteria may help improve this channel, but nevertheless the dijet channel is not promising.

We are particularly interested in the third generation final states. Heavy quark tagging techniques make it possible to observe these channels. Moreover, they can determine the (family universal) Z' couplings to up-type quarks and down-type quarks. In the case that

⁹In principle the mass could be determined indirectly, e.g., by comparing results from the ILC at different energies. However, the ILC sensitivity is small for a multi-TeV Z' mass.

¹⁰The uncertainties in $\Gamma_{Z'}$ are too large to obtain useful model-independent constraints from $\sigma^e \Gamma_{Z'}$.

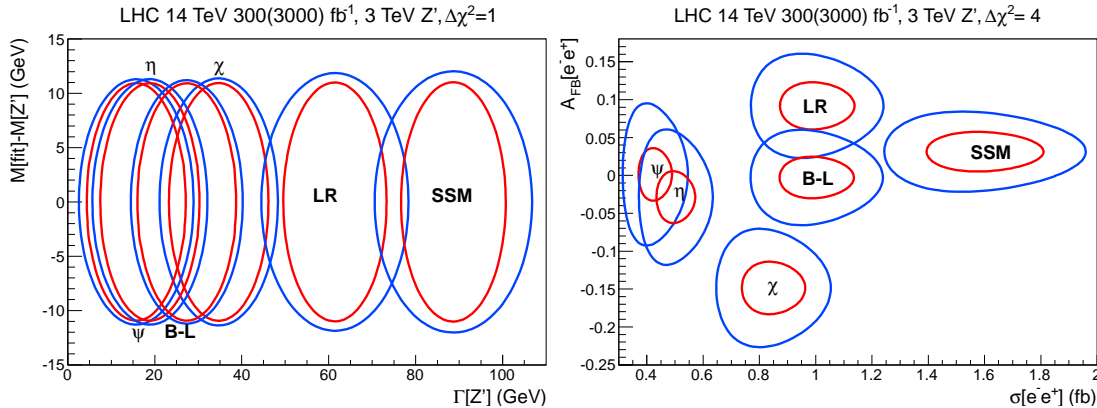


Figure 2. The results for $pp \rightarrow Z' \rightarrow e^- e^+$ with dielectron invariant mass from 2.8 – 3.2 TeV. *Left panel:* $\Delta\chi^2 = 1$ contours for the fitted width versus mass for the LHC at 300 fb^{-1} and 3000 fb^{-1} . *Right panel:* $\Delta\chi^2 = 4$ contours of the simulated forward-asymmetry versus the cross section.

top quark charge and/or polarization tagging is available, one would be able to obtain constraints on the chiral couplings of the Z' . On the other hand, the top quark signal is statistically very limited, as shown in the table. The top tagging and mis-tagging rates in this highly boosted scenario require further investigation. Thus we only list its parton level cross section and not discuss backgrounds.

	χ	ψ	η	LR	B-L	SSM
σ_{2j}^{SM} (fb)	1.4×10^6					
$\sigma_{2j;\text{cut}}^{SM}$ (fb)	5.1×10^3					
$\sigma_{2j}^{Z'}$ (fb)	6.0	5.6	8.3	21	1.4	19
$\sigma_{2b}^{Z'}$ (fb)	2.9	1.6	1.9	7.8	0.4	6.2
$\sigma_{2b}^{SM+Z'}$ (fb)	5.5	3.7	3.9	10	2.3	8.7
$\sigma_{2t}^{Z'}$ (fb)	0.7	1.7	3.2	5.8	0.5	7.0

Table 3. Parton level cross sections at the LHC 14 TeV. We only select events with final state dijet and bottom pair invariant mass in the window 2.9 – 3.1 TeV. $\sigma_{2j;\text{cut}}^{SM}$ are with cuts h_t (scalar sum of jets' p_{Tj}) > 500 GeV, $p_T > 200$ GeV, and $y_j < 2$.

For the bottom pair final state we include both the QCD dijet background and the SM bottom pair irreducible background. We show the cut flow effective acceptance ϵ and final significance at LHC 14 TeV in Table 4. The QCD dijets are required to be in the mass window of 2.5 – 3.5 TeV, with $h_t > 500$ GeV and leading jet $p_t > 200$ GeV at the parton level. The cross section is 36 pb, but tight b -tagging criteria that have a 0.1% fake rate from light quark jets can reduce it greatly. Both the signal and irreducible bottom pair background require $b\bar{b}$ invariant mass in the same window. The effective invariant mass m_{eff} is the invariant mass of all the jets with $p_t > 100$ GeV. After these series of cuts, we

	QCD Dijet	SM $b\bar{b}$	χ	ψ	η	LR	B-L	SSM
σ (fb)	36300	12.1	3.44	1.73	2.03	10.8	0.45	9.74
ϵ_b (%)	0.561	27.6	30.7	30.1	30.2	29.7	30.7	28.7
$\epsilon_{P_t^b}$ (%)	0.0365	6.80	9.07	9.14	9.34	8.15	9.56	7.63
σ_{eff} (fb)	11.78	0.82	0.31	0.16	0.19	0.88	0.04	0.74
$\frac{S}{\sqrt{B}} @ 0.3 \text{ ab}^{-1}$			1.5	0.8	0.9	4.3	0.2	3.6
$\frac{S}{\sqrt{B}} @ 3 \text{ ab}^{-1}$			4.8	2.4	2.9	14	0.7	11

Table 4. Cut flow table and significance S/\sqrt{B} for $Z' \rightarrow b\bar{b}$ processes at LHC 14 TeV. The cross sections σ before cuts are for bottom pair (dijet) invariant mass from 2.5 – 3.5 TeV. ϵ_b represents the percentage acceptance of at least one tagged b -jet. $\epsilon_{P_t^b}$ represents the percentage acceptance also requiring the p_T of the leading b -jet to be greater than 1.2 TeV. σ_{eff} is the cross section after these cuts.

will be able to establish three sigma significance for the excess for the benchmark models Z_χ , Z_{LR} and Z_{SSM} in the $b\bar{b}$ final state at LHC 14 TeV with 3000 fb^{-1} .

2.2 ILC Effects

A lepton collider with high luminosity could probe the Z' couplings through their interference with the SM. Here we study the sensitivity of different observables to a Z' at the 500 GeV and 1 TeV ILC. Previous studies include [18, 19, 22, 42–47].

We show our results in Figure 3. We apply an acceptance of polar angle for the charged leptons in region of $10^\circ < \theta < 170^\circ$ [48]. We require a minimal p_T of 20 GeV for jets. We include a 0.25% polarization uncertainty, 0.2% uncertainties on leptonic observables, and 0.5% uncertainties on hadronic observables [49]. Among those uncertainties associated with leptonic and hadronic final states, we assume that 0.14% are correlated and thus will cancel in asymmetry observables. The τ lepton, bottom quark, and top quark tagging efficiencies are set at 60%, 96% [49] and 70%.

We study the accuracies of the muon forward-backward asymmetry $A_{FB}[\mu^-\mu^+]$ and the cross section $\sigma[\mu^-\mu^+]$ for the dimuon final state¹¹, assuming the fixed (normal) beam polarization¹² $\mathcal{P}(e^-, e^+) = (+0.8, +0.3)$, using the formulae in (B.1) and (B.9). The muon forward-backward asymmetry in the SM is relatively large, as shown in the left panel of Figure 3. The difference in cross section is dominantly a summation of interference terms from different squared helicity amplitudes, and it is possible to have sizable interferences without changing the cross section much. A typical example is the Z'_{SSM} , shown in the figure, and similarly the Z'_{LR} . All of the leptonic cross sections are smaller than the SM. This is no longer true for hadronic final states, since $g_{L/R}^e g_{L/R}^{u/d}$ could have either sign. From this figure we can see that Z'_χ , Z'_{B-L} and Z'_{SSM} are well separated from the SM.

¹¹Dielectron final states also involve t -channel exchanges.

¹²As discussed in Appendix B.2 we define $\mathcal{P} > 0$ for predominantly left (right)-handed $e^-(e^+)$.

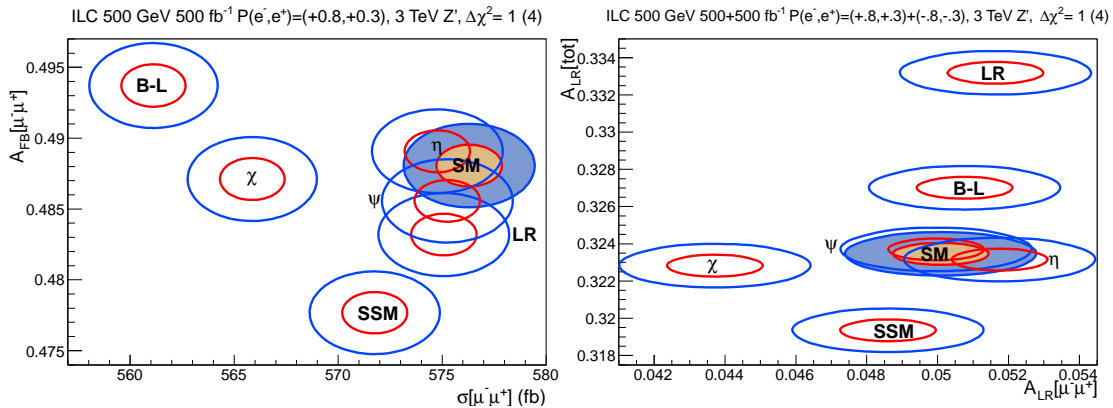


Figure 3. The accuracies of ILC observables for a 500 GeV ILC. Details of the assumed uncertainties are discussed in the text. *Left panel:* $\Delta\chi^2 = 1(4)$ contours (red (blue)) of the simulated $e^-e^+ \rightarrow \mu^-\mu^+$ cross sections $\sigma[\mu^-\mu^+]$ and the forward-backward asymmetry $A_{FB}[\mu^-\mu^+]$ in the dimuon system, with 500 fb^{-1} data at fixed beam polarization $P(e^-, e^+) = (+0.8, +0.3)$. *Right panel:* $\Delta\chi^2 = 1(4)$ contours (red (blue)) of the simulated polarization (left-right) asymmetry in the dimuon system $A_{LR}[\mu^-\mu^+]$, and the total polarization asymmetry $A_{LR}[tot]$ (including all of the final states except e^-e^+ and $\nu\bar{\nu}$), with 500 fb^{-1} each for beam polarizations $P(e^-, e^+) = (+0.8, +0.3)$ and $P(e^-, e^+) = (-0.8, -0.3)$.

If the beam polarization can be flipped from normal polarization to the reversed polarization $P(e^-, e^+) = (-0.8, -0.3)$, one can determine the polarization (left-right) asymmetry $A_{LR}[\mu^-\mu^+]$ for the dimuon channel, defined in (B.12) and (B.13), for which some of the systematics cancel. One can also observe the total polarization asymmetry $A_{LR}[tot]$ defined in (B.14), for which one does not need to identify the final state (other than removing the dielectron) and which has higher statistics. However, there are some cancellations between final states. For example, some final states may have positive deviations from the SM while others have negative deviations. Both $A_{LR}[\mu^-\mu^+]$ and $A_{LR}[tot]$ are shown in the right panel of Figure 3, assuming 500 fb^{-1} for each polarization¹³ For the $A_{LR}[tot]$, we sum all of the observed final states other than the dielectron¹⁴. A_{LR} has the merit that not only most of the luminosity uncertainty cancels, but also many systematic uncertainties, such as those associated with tagging efficiencies, acceptances, etc., cancel. Therefore, we only include the polarization and statistical uncertainties when treating the polarization asymmetries¹⁵. $A_{LR}[\mu^-\mu^+]$ is especially sensitive to Z'_χ , while $A_{LR}[tot]$ is useful for

¹³With the doubled run one would also have such new observables as $\sigma_L + \sigma_R$ in (B.12), A_{FB} in (B.9) with reversed polarization, or A_{LR}^{FB} in (B.15). Alternatively, one could divide a 500 fb^{-1} run into two 250 fb^{-1} runs with opposite polarizations, in which case the outer contours in Figure 3 would correspond to $\Delta\chi^2 = 2.6$.

¹⁴The major contribution to $A_{LR}[tot]$ is from the hadronic final states, since the polarization asymmetry for dileptons is much smaller. One could also consider different final states separately to gain better statistical sensitivity (but with larger systematic uncertainties).

¹⁵Some parametric uncertainties in the SM parameters don't cancel. We ignore them here as they are expected to improve in the future [50].

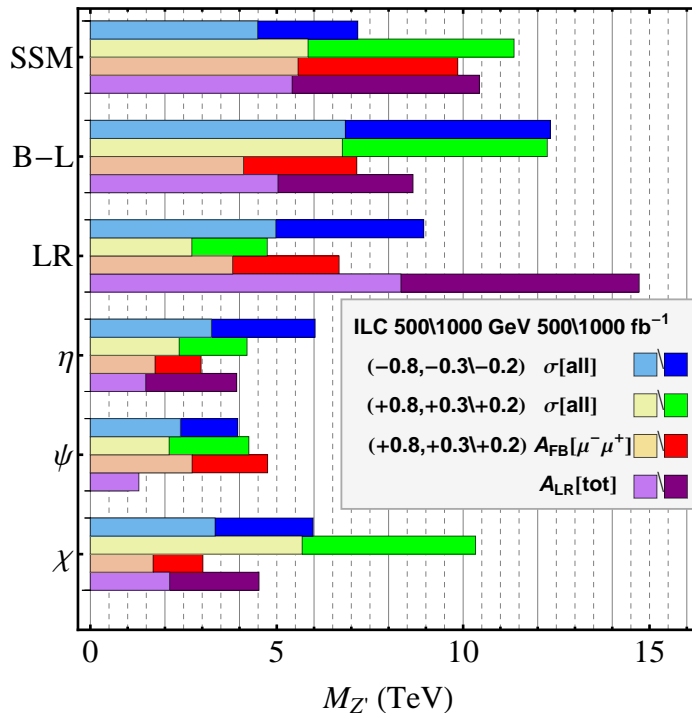


Figure 4. The exclusion reach of the 500 GeV (1 TeV) ILC with 500 fb^{-1} (1000 fb^{-1}) of integrated luminosity for both normal beam polarization $P(e^-, e^+) = (+0.8, +0.3)$ ($P(e^-, e^+) = (+0.8, +0.2)$) (brown (red) and yellow (green)) and reversed beam polarization $P(e^-, e^+) = (-0.8, -0.3)$ ($P(e^-, e^+) = (-0.8, -0.2)$) (cyan (blue)). We show the complementarities between different beam polarizations and observables σ including all channels other than the dielectron (cyan (blue) and yellow (green)) and A_{FB} from the dimuon final state (brown (red)). We also show the exclusion reach (magenta (purple)) from $A_{LR}[tot]$ for reversed beam polarizations, with $500 + 500 \text{ fb}^{-1}$ and $1000 + 1000 \text{ fb}^{-1}$ for the ILC 500 GeV and ILC 1000 GeV, respectively. The reaches from $A_{LR}[tot]$ would be reduced by $\sim 15\%$ for divided runs of $250 + 250 \text{ fb}^{-1}$ and $500 + 500 \text{ fb}^{-1}$.

distinguishing Z'_{LR} .

There is some complementarity between the LHC and ILC observations, as can be seen in Figures 2 and 3. For example, the LHC has limited discrimination between the LR, B-L, and SSM models, especially from the cleaner $A_{FB}[e^-e^+]$, while these could be well-separated using the ILC observables.

3 Case 2: Z' Beyond the LHC Reach

We show the exclusion (95% C.L.) reach of the ILC at 500 GeV and 1 TeV, including the case that the Z' is beyond the LHC reach, in Figure 4. We show the reach from both the normal and reversed beam polarizations obtained from the cross sections for $\mu^-\mu^+, \tau^-\tau^+$, 2 jets (from light quarks), $b\bar{b}$, and $t\bar{t}$, where we combine the χ^2 from each channel after including the appropriate systematic uncertainties. We also show the exclusion reach from

the muon forward-backward asymmetry $A_{FB}[\mu^-\mu^+]$ and from $A_{LR}[tot]$. In the latter case we assume that the beam polarizations can be reversed and that a full luminosity run is made for each polarization. The uncertainties included are described in the previous section. We assume the deviations in the cross sections and asymmetries from the SM scale with $M_{Z'}^{-2}$. We conservatively estimate that corrections will reduce the exclusion reach by $\lesssim 2\%$. There is no single best exclusion observable; for some models like Z'_χ and Z'_{SSM} the normal polarization is better, for others like Z'_ψ , Z'_η and Z'_{LR} the reversed beam polarization or the forward-backward asymmetry has a larger reach. The polarization asymmetries, with a portion of systematic uncertainties cancelled, is especially stringent for the LR model.

4 Conclusions

We study and discuss the Z' discovery and model discrimination potential of the LHC and ILC, using the benchmark models Z'_χ , Z'_ψ , Z'_η , Z'_{LR} , Z'_{B-L} , and Z'_{SSM} . We discuss two scenarios: (1) a 3 TeV Z' that can be resonantly produced at the LHC; (2) a Z' that is too massive to observe as a clear resonance signal.

We discuss the potential of the LHC at 14 TeV with integrated luminosity of 300 fb^{-1} and 3000 fb^{-1} in both leptonic and hadronic final states. The leptonic final states have low background and provide the best sensitivity for discovery. The excellent lepton energy resolution allows them to probe the Z' mass and width. We show in the left panel of Figure 2 that for 300 fb^{-1} (and 3000 fb^{-1}), one can reach around 10 GeV precision for each at $\sim 1\sigma$. Unfortunately, the width uncertainty is a significant fraction of the width itself for typical models with electroweak-scale couplings, limiting the possibility of constraining the absolute magnitudes of the couplings. The leptonic forward-backward asymmetry, combined with the cross section would have some sensitivity to the chiral couplings, and in particular would allow discrimination between benchmark models (with minimal width) at a reasonable level. We also discuss the hadronic Z' modes at the LHC. We study the sensitivity of the bottom pair final state in detail. Although there is a large background from mis-tagged light jets as shown in Table 4, a 3σ excess can be achieved for certain benchmark models, such as Z'_χ , Z'_{LR} and Z'_{SSM} .

For the ILC, the chiral couplings and Z' mass affect various observables through the interference of the Z' with SM contributions. Typical observables include the cross section σ , forward-backward asymmetry A_{FB} for di-fermion systems with charge identification, and polarization asymmetries A_{LR} for reversed beam polarizations. (Other possibilities include the polarized forward-backward asymmetry and the final state polarizations in $\tau^+\tau^-$ and $t\bar{t}$.) We show the cross section and forward-backward asymmetry for the dimuon system in the left panel of Figure 3. It shows good discrimination potential for Z'_χ , Z'_{B-L} and Z'_{SSM} from other models and the SM background. The polarization asymmetry for the total (except for dielectron) cross section and the dimuon final states are also potentially very useful if the e^\mp polarizations can be reversed, as shown in the right panel of Figure 3. The asymmetry for the total cross section is especially important because it involves high

statistics and reduced systematic uncertainties, since the final states do not need to be identified.

For the scenarios in which the Z' cannot be resonantly produced, we study the exclusion reach for the ILC from cross sections, forward-backward asymmetries, and polarization asymmetries. The results are shown in Figure 4, which also shows the complementarity between these observables.

In this preliminary study we have focused on the ability of various observables at the LHC and ILC to discriminate between several benchmark Z' models with minimal width. For $M_{Z'} \sim 3$ TeV the LHC should be able to observe a Z' through its leptonic decays, and obtain a measurement of its mass and width at the 10 GeV level. Some sensitivity to the chiral couplings (as illustrated by model discrimination) would be possible at the LHC and especially at the ILC, and the ILC reach would extend considerably higher as well.

However, there are a very large variety of possible models, including those with much weaker or stronger couplings than our benchmarks. Ideally, one would like to obtain as much information as possible in a model-independent way from the LHC, ILC, other colliders, and also from existing and future precision electroweak experiments. The inclusion of additional observables (such as heavy particle final states, additional asymmetries and polarizations, and precision electroweak constraints), a global χ^2 study for model discrimination, the possibility of model-independent coupling extractions, and the implications of departing from such assumptions as family universality are under investigation.

Acknowledgments

We are grateful to Chip Brock and Steve Godfrey for useful discussions. T.H. and Z.L. are supported in part by the U.S. Department of Energy under Grant No. DE-FG02-95ER40896, and in part by the PITT PACC. Z.L. is also supported in part by the LHC Theory Initiative from the U.S. National Science Foundation under Grant No. NSF-PHY-0969510. L.T.W. is supported by the NSF under grant PHY-0756966 and the DOE Early Career Award under grant. de-sc0003930. This work was supported in part by the National Science Foundation under Grant No. PHYS-1066293 and the hospitality of the Aspen Center for Physics.

Appendices

A Z' at the LHC

Here we establish our notation and summarize the basic formalism for the production and decay of a Z' into a fermion pair at the LHC by the process $p_A p_B \rightarrow f \bar{f} + X$. We define $s = (p_A + p_B)^2$ and $\hat{s} = (p_f + p_{\bar{f}})^2$, where in our examples we take $s = (14 \text{ TeV})^2$ and $\hat{s} = (3 \text{ TeV})^2$. y is the $f \bar{f}$ rapidity, with $y > 0$ along the \vec{p}_A direction (i.e., the $f \bar{f}$ boost direction). θ^* is the angle of f in the $f \bar{f}$ rest frame, defined¹⁶ with respect to y (i.e., with

¹⁶The θ^* convention is opposite that in [15] for $y < 0$, which was motivated by the simultaneous study of $p\bar{p}$.

respect to \vec{p}_A for $y > 0$ and \vec{p}_B for $y < 0$), and $z = \cos\theta^*$. We ignore the transverse momentum p_T of the $f\bar{f}$ system.

Let $f_{q_i}(x)[f_{\bar{q}_i}(x)]$ be the proton PDF of the i^{th} flavor quark [antiquark] q_i [\bar{q}_i], evaluated at the scale μ^2 , which we will take to be \hat{s} . The tree-level cross section for Drell-Yan production is then

$$\frac{d\sigma}{d\hat{s} dy dz} = \frac{1}{\hat{s}} \sum_{i=u,d,c,s,b} \left[p_i(\hat{s}, y) \frac{d\sigma(q_i \bar{q}_i \rightarrow f\bar{f})}{dz} + \bar{p}_i(\hat{s}, y) \frac{d\sigma(\bar{q}_i q_i \rightarrow f\bar{f})}{dz} \right], \quad (\text{A.1})$$

where¹⁷

$$p_i(\hat{s}, y) \equiv x_A x_B f_{q_i}(x_A) f_{\bar{q}_i}(x_B), \quad \bar{p}_i(\hat{s}, y) \equiv x_A x_B f_{\bar{q}_i}(x_A) f_{q_i}(x_B), \quad (\text{A.2})$$

with

$$x_{A,B} \equiv \sqrt{\frac{\hat{s}}{s}} e^{\pm y}. \quad (\text{A.3})$$

For family-independent couplings and ignoring quark masses, we can absorb the heavier quark PDFs into $p_{u,d}$, i.e., we redefine $p_u + p_c \rightarrow p_u$ and $p_d + p_s + p_b \rightarrow p_d$, and similarly for $\bar{p}_{u,d}$, with $\sum_{i=u,d,c,s,b} \rightarrow \sum_{i=u,d}$. We also define the distribution functions integrated over rapidity

$$P_i(\hat{s}, y_1, y_2) = \int_{y_1}^{y_2} p_i(\hat{s}, y) dy, \quad \bar{P}_i(\hat{s}, y_1, y_2) = \int_{y_1}^{y_2} \bar{p}_i(\hat{s}, y) dy, \quad (\text{A.4})$$

where $0 \leq y_1 < y_2 \leq y_{\text{max}}$.

The differential cross sections in (A.1) due to s -channel γ, Z , and Z' are given by

$$\frac{d\sigma(q_i \bar{q}_i \rightarrow f\bar{f})}{dz} = \frac{C_f}{384\pi\hat{s}} \{ [G_{LL}^i + G_{RR}^i] (1+z)^2 + [G_{LR}^i + G_{RL}^i] (1-z)^2 \}, \quad (\text{A.5})$$

where C_f is the color factor (1 for leptons and 3 for quarks), and¹⁸

$$G_{ab}^i(\hat{s}) = \left| e^2 q^i q^f + \frac{g_a^{1i} g_b^{1f} \hat{s}}{\hat{s} - M_Z^2 + iM_Z \Gamma_Z} + \frac{g_a^{2i} g_b^{2f} \hat{s}}{\hat{s} - M_{Z'}^2 + iM_{Z'} \Gamma_{Z'}} \right|^2 \quad (\text{A.6})$$

for $a, b = L, R$. The expression for $\frac{d\sigma(\bar{q}_i q_i \rightarrow f\bar{f})}{dz}$ is the same except $(1 \pm z)^2 \rightarrow (1 \mp z)^2$. We have ignored the masses of the initial and final fermions in (A.5), which is an adequate approximation except for the t quark. For our simulations, the top quarks mass is approximately included. The massive top quark will also affect the top charge tagging efficiency through its leptonic decays. For simplicity, we will evaluate the SM couplings for both the LHC and ILC cases at M_Z .

¹⁷Higher order QCD K factors $K(\hat{s}, y)$ can be included in p_i and \bar{p}_i . We have not implemented the K factors in the present study. They will potentially increase the sensitivity through an increase in cross section, and may alter the angular distribution slightly.

¹⁸ G_{ab}^i and the analogous C_{ab}^i defined in (A.9) should more properly be written as G_{ab}^{if} and C_{ab}^{if} , respectively. We usually suppress the dependence on the final state fermion for notational simplicity.

Near the Z' pole it is often adequate to ignore the γ and Z , in which case

$$G_{ab}^i(\hat{s}) \rightarrow \hat{s}^2 |D(\hat{s})|^2 C_{ab}^i, \quad (\text{A.7})$$

where

$$|D(\hat{s})|^2 = \frac{1}{(\hat{s} - M_{Z'}^2)^2 + M_{Z'}^2 \Gamma_{Z'}^2}, \quad (\text{A.8})$$

is the Breit-Wigner propagator-squared and

$$C_{ab}^i \equiv |g_a^i|^2 |g_b^i|^2, \quad a, b = L, R. \quad (\text{A.9})$$

A.1 Narrow Width Approximation

We first consider Z' production, ignoring interference effects, in the narrow width approximation (NWA),

$$|D(\hat{s})|^2 \rightarrow \frac{\pi}{M_{Z'} \Gamma_{Z'}} \delta(\hat{s} - M_{Z'}^2). \quad (\text{A.10})$$

This is a reasonable first approximation for a multi-TeV scale Z' with electroweak couplings, for which typically $\Gamma_{Z'}/M_{Z'} = \mathcal{O}(1\%)$ unless there are important non-SM decay channels.

The cross section is then

$$\begin{aligned} \frac{d\sigma}{dy dz} &\rightarrow \frac{C_f}{384 M_{Z'} \Gamma_{Z'}} \sum_{i=u,d} \{ [p_i C_N^i + \bar{p}_i C_F^i] (1+z)^2 + [p_i C_F^i + \bar{p}_i C_N^i] (1-z)^2 \} \\ &= \frac{C_f}{384 M_{Z'} \Gamma_{Z'}} \sum_{i=u,d} \{ p_i^+ C_+^i (1+z^2) + 2p_i^- C_-^i z \}, \end{aligned} \quad (\text{A.11})$$

where

$$p_i^\pm \equiv p_i \pm \bar{p}_i, \quad P_i^\pm \equiv P_i \pm \bar{P}_i, \quad (\text{A.12})$$

and

$$\begin{aligned} C_N^i &\equiv C_{LL}^i + C_{RR}^i, & C_F^i &\equiv C_{LR}^i + C_{RL}^i \\ C_\pm^i &\equiv C_N^i \pm C_F^i = (C_{LL}^i + C_{RR}^i) \pm (C_{LR}^i + C_{RL}^i). \end{aligned} \quad (\text{A.13})$$

Integrating over angles (one could include a cut on maximum $|z|$):

$$\begin{aligned} \frac{d\sigma}{dy} &= \int_{-1}^{+1} \frac{d\sigma}{dy dz} dz = \frac{C_f}{144 M_{Z'} \Gamma_{Z'}} \{ p_u^+ C_+^u + p_d^+ C_+^d \} \\ \sigma &= \left(\int_{y_1}^{y_2} + \int_{-y_2}^{-y_1} \right) \frac{d\sigma}{dy} dy = \frac{C_f}{72 M_{Z'} \Gamma_{Z'}} \{ P_u^+ C_+^u + P_d^+ C_+^d \}. \end{aligned} \quad (\text{A.14})$$

These results are sometimes rewritten in terms of the Z' partial widths

$$\begin{aligned} \Gamma(Z' \rightarrow f\bar{f}) &= \frac{C_f M_{Z'}}{24\pi} (|g_L^f|^2 + |g_R^f|^2) \\ \Gamma(Z' \rightarrow q_i \bar{q}_i) &= \frac{M_{Z'}}{8\pi} (|g_L^i|^2 + |g_R^i|^2), \end{aligned} \quad (\text{A.15})$$

so that

$$\frac{d\sigma}{dy} = \frac{4\pi^2}{3M_{Z'}^3} [p_u^+ \Gamma(Z' \rightarrow u\bar{u}) + p_d^+ \Gamma(Z' \rightarrow d\bar{d})] B(Z' \rightarrow f\bar{f}), \quad (\text{A.16})$$

where $B(Z' \rightarrow f\bar{f}) \equiv \Gamma(Z' \rightarrow f\bar{f})/\Gamma_{Z'}$ is the branching ratio into $f\bar{f}$. Similarly,

$$\sigma \equiv \sigma_{Z'} B(Z' \rightarrow f\bar{f}) = \frac{8\pi^2}{3M_{Z'}^3} [P_u^+ \Gamma(Z' \rightarrow u\bar{u}) + P_d^+ \Gamma(Z' \rightarrow d\bar{d})] B(Z' \rightarrow f\bar{f}) \quad (\text{A.17})$$

is the total cross section into $f\bar{f}$. (We will sometimes denote σ by σ^f or by $\sigma[f\bar{f}]$.) Since $\Gamma_{Z'}$ is not known a priori (except in specific models) one cannot directly constrain the absolute couplings from σ^f , although one can obtain ratios of couplings by comparing different final states. However, if $\Gamma_{Z'}$ can be measured independently from the lineshape to a precision of around 25 GeV as shown in the left panel of Figure 3, then $\sigma^f \Gamma_{Z'} = \sigma_{Z'} \Gamma(Z' \rightarrow f\bar{f})$ does contains information on the absolute couplings. Another difficulty is that the cross section for a given f depends on the combination $C_+^u + C_+^d (P_d^+ / P_u^+)$. In principle, one could separate $C_{u,d}^+$ by using the rapidity dependence, but in practice there is little sensitivity for $M_{Z'} \gtrsim 3$ TeV. (Similar statements apply to the rapidity dependence of the angular distribution.) The u and d couplings could, however, be separated if one can observe $b\bar{b}$ and $t\bar{t}$ (assuming family-universality).

In addition to $\Gamma_{Z'}$, the total cross sections suffer from PDF, luminosity, K factor, and other systematic uncertainties. These difficulties are reduced for ratios of rates for different final states, angular distributions, and final state polarizations.

A.2 Angular Distribution

Define the forward (F) and backward (B) cross sections for rapidity y as

$$F(y) \equiv \int_0^1 \frac{d\sigma}{dy dz} dz, \quad B(y) \equiv \int_{-1}^0 \frac{d\sigma}{dy dz} dz. \quad (\text{A.18})$$

Recall that positive z corresponds to f in the direction of the rapidity, so that F and B are symmetric under $y \rightarrow -y$. It is also useful to define F and B integrated over a range of $|y|$:

$$F \equiv \left(\int_{y_1}^{y_2} + \int_{-y_2}^{-y_1} \right) F(y) dy, \quad B \equiv \left(\int_{y_1}^{y_2} + \int_{-y_2}^{-y_1} \right) B(y) dy. \quad (\text{A.19})$$

The forward-backward asymmetries are then

$$A_{FB}(y) \equiv \frac{F(y) - B(y)}{F(y) + B(y)} = \frac{3}{4} \frac{p_u^- C_-^u + p_d^- C_-^d}{p_u^+ C_+^u + p_d^+ C_+^d} \quad (\text{A.20})$$

$$A_{FB} \equiv \frac{F - B}{F + B} = \frac{3}{4} \frac{P_u^- C_-^u + P_d^- C_-^d}{P_u^+ C_+^u + P_d^+ C_+^d},$$

for which the $\Gamma_{Z'}$, luminosity, and some of the PDF uncertainties cancel. Of course, $A_{FB}(0) = 0$ for pp since $p_-^i = 0$, but $A_{FB}(y)$ can be nonzero for $y \neq 0$ [15]. For large positive y , for example, the cross section is dominated by $q_i \bar{q}_i$, with little dilution from $\bar{q}_i q_i$, leading to the possibility of a large asymmetry. Of course, the cross section is smaller at high y , so that one should try to optimize the $y_{1,2}$ range.

The forward-backward asymmetry is equivalent to the charge asymmetry A_c defined by

$$A_{FB} = A_c \equiv \frac{\sigma(|y_f| > |y_{\bar{f}}|) - \sigma(|y_f| < |y_{\bar{f}}|)}{\sigma(|y_f| > |y_{\bar{f}}|) + \sigma(|y_f| < |y_{\bar{f}}|)}, \quad (\text{A.21})$$

at least in the absence of cuts.

A.3 Final State Polarization

One can also consider final state polarizations¹⁹, defined as

$$P_f = \frac{\sigma^{fR} - \sigma^{fL}}{\sigma^{fR} + \sigma^{fL}}, \quad (\text{A.22})$$

where σ^{fR} and σ^{fL} are respectively the rates for producing right and left-helicity f .

In addition to (A.13) it is convenient to define the combinations

$$\begin{aligned} C_L^i &\equiv C_{LL}^i + C_{LR}^i, & C_R^i &\equiv C_{RL}^i + C_{RR}^i \\ \hat{C}_L^i &\equiv C_{LL}^i - C_{LR}^i, & \hat{C}_R^i &\equiv C_{RL}^i - C_{RR}^i, \end{aligned} \quad (\text{A.23})$$

and

$$\begin{aligned} C_P^i &\equiv C_L^i - C_R^i = C_{LL}^i - C_{RR}^i + C_{LR}^i - C_{RL}^i \\ \hat{C}_P^i &\equiv \hat{C}_L^i - \hat{C}_R^i = C_{LL}^i - C_{RR}^i - C_{LR}^i + C_{RL}^i, \end{aligned} \quad (\text{A.24})$$

with

$$C_L^i + C_R^i = \hat{C}_L^i + \hat{C}_R^i = C_N^i + C_F^i = C_+^i. \quad (\text{A.25})$$

Then, ignoring the mass of f ,

$$P_f = - \frac{\sum_{i=u,d} \{ p_i^+ \hat{C}_P^i (1+z^2) + 2p_i^- C_P^i z \}}{\sum_{i=u,d} \{ p_i^+ C_+^i (1+z^2) + 2p_i^- C_-^i z \}}. \quad (\text{A.26})$$

One can integrate the numerator and denominator separately over the desired ranges of y and z . The polarization of \bar{f} is opposite to that of f for $m_f \sim 0$.

A.4 Beyond the Narrow Width Approximation

Define the combinations $G_{N,F}^i, G_{\pm}^i, G_{L,R}^i, \hat{G}_{L,R}^i, G_P^i$, and \hat{G}_P^i of the parameters $G_{ab}^i(\hat{s})$ in (A.6) in analogy with the combinations of C_{ab}^i in (A.13), (A.23), and (A.24). Then

$$\begin{aligned} \frac{d\sigma}{d\hat{s} dy dz} &= \frac{C_f}{384\pi\hat{s}^2} \sum_{i=u,d} \{ [p_i G_N^i + \bar{p}_i G_F^i] (1+z)^2 + [p_i G_F^i + \bar{p}_i G_N^i] (1-z)^2 \} \\ &= \frac{C_f}{384\pi\hat{s}^2} \sum_{i=u,d} \{ p_i^+ G_+^i (1+z^2) + 2p_i^- G_-^i z \}, \end{aligned} \quad (\text{A.27})$$

¹⁹Here we list just the polarizations. In practice, it might be best to consider the actual observables that depend on the polarization, i.e., the angular distributions of the f and \bar{f} decay products.

Other relevant observables (for $m_f = 0$) are then

$$\begin{aligned}
\frac{d\sigma}{d\hat{s} dz} &= \frac{C_f}{192\pi\hat{s}^2} \sum_{i=u,d} \{P_i^+ G_+^i (1+z^2) + 2P_i^- G_-^i z\} \\
\frac{d\sigma}{d\hat{s} dy} &= \frac{C_f}{144\pi\hat{s}^2} \{p_u^+ G_+^u + p_d^+ G_+^d\} \\
\frac{d\sigma}{d\sqrt{\hat{s}}} &= 2\sqrt{\hat{s}} \frac{d\sigma}{d\hat{s}} = \frac{C_f}{36\pi\hat{s}^{3/2}} \{P_u^+ G_+^u + P_d^+ G_+^d\} \\
A_{FB}(\hat{s}, y) &= \frac{3}{4} \frac{p_u^- G_-^u + p_d^- G_-^d}{p_u^+ G_+^u + p_d^+ G_+^d} \\
P_f &= -\frac{\sum_{i=u,d} \{p_i^+ \hat{G}_P^i (1+z^2) + 2p_i^- G_P^i z\}}{\sum_{i=u,d} \{p_i^+ G_+^i (1+z^2) + 2p_i^- G_-^i z\}}.
\end{aligned} \tag{A.28}$$

One can separately integrate the numerator and denominator of A_{FB} over the desired ranges of \hat{s} and y to obtain the integrated asymmetry. Similarly, the numerator and denominator of P_f can be separately integrated over the desired ranges of \hat{s} , y , and z . The polarization of \bar{f} is opposite to that of f for $m_f \sim 0$.

A.5 Finite Mass Corrections

B Z' at the ILC

We now consider $e^- e^+ \rightarrow f \bar{f}$ at CM energy \sqrt{s} . The final fermion f can be μ, τ, b, t or possibly c, s , or unidentified quark. (We do not consider $f = e$ because that involves t channel exchange as well as s channel.) Define

$$G_{ab}^e(s) = \left| e^2 q^e q^f + \frac{g_a^{1e} g_b^{1f} s}{s - M_Z^2 + iM_Z \Gamma_Z} + \frac{g_a^{2e} g_b^{2f} s}{s - M_{Z'}^2 + iM_{Z'} \Gamma_{Z'}} \right|^2, \tag{B.1}$$

in analogy to (A.6). We assume $M_Z \ll \sqrt{s} \ll M_{Z'}$, so we can ignore Γ_Z and $\Gamma_{Z'}$.

B.1 No Polarization

In the absence of polarization for the e^\mp the observables are

$$\begin{aligned}
\frac{d\sigma(s)}{dz} &= \frac{C_f}{128\pi s} \{[G_{LL}^e + G_{RR}^e] (1+z)^2 + [G_{LR}^e + G_{RL}^e] (1-z)^2\} \\
&= \frac{C_f}{128\pi s} \{G_+^e (1+z^2) + 2G_-^e z\} \\
\sigma(s) &= \frac{C_f}{48\pi s} G_+^e \\
A_{FB}(s) &= \frac{3}{4} \frac{G_-^e}{G_+^e} \\
P_f &= -\frac{\hat{G}_P^e (1+z^2) + 2G_P^e z}{G_+^e (1+z^2) + 2G_-^e z},
\end{aligned} \tag{B.2}$$

where the various G_{ab}^e combinations are defined in analogy to the combinations of C_{ab}^i in (A.13), (A.23), and (A.24). As usual, one can integrate numerator and denominator of P_f over z to obtain the average polarization $P_f = -\hat{G}_P^e/G_+^e$.

Although we are mainly concerned with the regime $M_Z \ll \sqrt{s} \ll M_{Z'}$ it is nevertheless useful to display the asymmetries and polarizations at the Z or Z' pole, ignoring interferences. For $s = M_Z^2$,

$$\begin{aligned} A_{FB}(M_Z^2) &\rightarrow \frac{3}{4} A_e^1 A_f^1 \\ P_f(M_Z^2) &\rightarrow -\frac{A_f(1+z^2) + 2A_e z}{(1+z^2) + 2A_e A_f z} \rightarrow -A_f^1 \end{aligned} \quad (\text{B.3})$$

with

$$A_f^1 \equiv \frac{(g_L^{1f})^2 - (g_R^{1f})^2}{(g_L^{1f})^2 + (g_R^{1f})^2} = \frac{2g_V^{1f} g_A^{1f}}{(g_V^{1f})^2 + (g_A^{1f})^2}. \quad (\text{B.4})$$

The second form for P_f is the average polarization. Similar expressions hold at the Z' pole, with $A_f^1 \rightarrow A_f^2$ and $g_a^{1f} \rightarrow g_a^{2f}$.

B.2 Fixed Initial State Polarization

For V and A interactions (and ignoring m_e), only the combinations $e_L^- e_R^+$ and $e_R^- e_L^+$ contribute yield nonzero amplitudes (unlike, S, P , and T , which are sensitive to $e_L^- e_L^+$ and $e_R^- e_R^+$). We define the initial state polarizations

$$\mathcal{P}^- = \eta_L^- - \eta_R^-, \quad \mathcal{P}^+ = \eta_R^+ - \eta_L^+, \quad (\text{B.5})$$

where η_L^- and $\eta_R^- = 1 - \eta_L^-$ are respectively the fractions of L and R -helicity e^- , and similarly for e^+ . Note that (neglecting m_e) $\mathcal{P}^- = \mathcal{P}^+ \sim 1$ for e^\mp produced in weak charge current processes. Also note that the definition of \mathcal{P}^- is conventional for $e^- e^+$, though it is opposite in sign from usual polarization definitions. Some useful relations are

$$\eta_{L,R}^- = \frac{1 \pm \mathcal{P}^-}{2}, \quad \eta_{L,R}^+ = \frac{1 \mp \mathcal{P}^+}{2} \quad (\text{B.6})$$

$$\frac{\eta_L^- \eta_R^+}{\eta_L^- \eta_R^+ + \eta_R^- \eta_L^+} = \frac{1 + \mathcal{P}_{eff}}{2}, \quad \frac{\eta_R^- \eta_L^+}{\eta_L^- \eta_R^+ + \eta_R^- \eta_L^+} = \frac{1 - \mathcal{P}_{eff}}{2}, \quad (\text{B.7})$$

where the effective polarization is defined as

$$\mathcal{P}_{eff} \equiv \frac{\mathcal{P}^- + \mathcal{P}^+}{1 + \mathcal{P}^- \mathcal{P}^+} = \frac{\eta_L^- \eta_R^+ - \eta_R^- \eta_L^+}{\eta_L^- \eta_R^+ + \eta_R^- \eta_L^+}. \quad (\text{B.8})$$

For example, $\mathcal{P}^- = 0.80$ and $\mathcal{P}^+ = 0.30$ yields $\mathcal{P}_{eff} \sim 0.89$, while $(\mathcal{P}^-, \mathcal{P}^+) = (0.80, 0.60) \Rightarrow \mathcal{P}_{eff} \sim 0.95$.

The relevant observables for fixed polarizations are

$$\begin{aligned}
\frac{d\sigma}{dz} &= \frac{C_f}{32\pi s} \left\{ [\eta_L^- \eta_R^+ G_{LL}^e + \eta_R^- \eta_L^+ G_{RR}^e] (1+z)^2 \right. \\
&\quad \left. + [\eta_L^- \eta_R^+ G_{LR}^e + \eta_R^- \eta_L^+ G_{RL}^e] (1-z)^2 \right\} \\
\sigma &= \frac{C_f}{12\pi s} [\eta_L^- \eta_R^+ G_L^e + \eta_R^- \eta_L^+ G_R^e] \\
A_{FB} &= \frac{3}{4} \frac{G_-^e + \mathcal{P}_{eff} \hat{G}_P^e}{G_+^e + \mathcal{P}_{eff} G_P^e} \rightarrow \frac{3}{4} A_f \frac{A_e + \mathcal{P}_{eff}}{1 + \mathcal{P}_{eff} A_e} \\
P_f &= - \frac{[\hat{G}_P^e + \mathcal{P}_{eff} G_-^e] (1+z^2) + 2[G_P^e + \mathcal{P}_{eff} G_+^e] z}{[G_+^e + \mathcal{P}_{eff} G_P^e] (1+z^2) + 2[G_-^e + \mathcal{P}_{eff} \hat{G}_P^e] z} \\
&\rightarrow - \frac{[A_f + \mathcal{P}_{eff} A_e A_f] (1+z^2) + 2[A_e + \mathcal{P}_{eff}] z}{[1 + \mathcal{P}_{eff} A_e] (1+z^2) + 2[A_e A_f + \mathcal{P}_{eff} A_f] z} \\
&\rightarrow -A_f.
\end{aligned} \tag{B.9}$$

The second forms for A_{FB} and P_f are valid at the Z or Z' pole (the superscript 1 or 2 on $A_{e,f}$ is implied). The third form for P_f is obtained by integrating the numerator and denominator over z .

B.3 Polarization Asymmetries

Denote the cross sections for the polarizations \mathcal{P}^\mp defined in the previous section by σ_L , and let σ_R represent the cross section for reversed polarizations

$$\eta_{L,R}^- \rightarrow \bar{\eta}_{L,R}^-, \quad \eta_{L,R}^+ \rightarrow \bar{\eta}_{L,R}^+, \tag{B.10}$$

with

$$\bar{\eta}_{L,R}^- = \eta_{R,L}^-, \quad \bar{\eta}_{L,R}^+ = \eta_{R,L}^+, \tag{B.11}$$

so that $\mathcal{P}^\mp \rightarrow -\mathcal{P}^\mp$. For example,

$$\begin{aligned}
\sigma_L &= \frac{C_f}{12\pi s} \{ \eta_L^- \eta_R^+ G_L^e + \eta_R^- \eta_L^+ G_R^e \} \\
\sigma_R &= \frac{C_f}{12\pi s} \{ \bar{\eta}_L^- \bar{\eta}_R^+ G_L^e + \bar{\eta}_R^- \bar{\eta}_L^+ G_R^e \} = \frac{C_f}{12\pi s} \{ \eta_R^- \eta_L^+ G_L^e + \eta_L^- \eta_R^+ G_R^e \}.
\end{aligned} \tag{B.12}$$

For $\mathcal{P}^\pm = 0$ these both reduce to the unpolarized cross section σ .

The polarization (left-right) asymmetry is defined as

$$A_{LR} \equiv \frac{\sigma_L - \sigma_R}{\sigma_L + \sigma_R} = \mathcal{P}_{eff} \frac{G_P^e}{G_+^e} \rightarrow \mathcal{P}_{eff} A_e, \tag{B.13}$$

where the second form is valid on the Z or Z' pole. (At the pole, A_{LR} is independent of the final state, allowing the determination of A_e from the total cross section polarization asymmetry.) It is also useful to define the total polarization asymmetry

$$A_{LR}^{tot} \equiv \frac{\sigma_L^{tot} - \sigma_R^{tot}}{\sigma_L^{tot} + \sigma_R^{tot}} = \mathcal{P}_{eff} \frac{\sum_f C_f G_P^{ef}}{\sum_f C_f G_+^{ef}} \rightarrow \mathcal{P}_{eff} A_e, \tag{B.14}$$

where we have added the superscript to emphasize the final state f . The sum can be taken over $f = \mu, \tau, u, d, c, s, b$, and t (if one ignores m_t). A_{LR}^{tot} is convenient in that one does not have to identify the final state (other than removing $f = e$, which also has t -channel contributions) and because one therefore has much higher statistics. However, the asymmetries between different final states may partially cancel away from the poles.

Assuming that the e^- and e^+ polarizations can each be turned off or reversed without affecting the magnitudes, one could in principle determine G_P^e/G_+^e (or the analogous quantity in (B.14)), \mathcal{P}_{eff} , \mathcal{P}^- , and \mathcal{P}^+ experimentally by measuring the asymmetries obtained by reversing the polarizations ($\mathcal{P}^-, \mathcal{P}^+$), ($\mathcal{P}^-, 0$), and ($0, \mathcal{P}^+$) (the Blondel scheme [51]).

Another useful observable is the left-right forward-backward asymmetry

$$A_{LR}^{FB} \equiv \frac{F_L - B_L - F_R + B_R}{F_L + B_L + F_R + B_R} = \frac{3}{4} \mathcal{P}_{eff} \frac{\hat{G}_P^e}{G_+^e} \rightarrow \frac{3}{4} \mathcal{P}_{eff} A_f, \quad (\text{B.15})$$

where

$$F_{L,R} \equiv \int_0^1 \frac{d\sigma_{L,R}}{dz} dz, \quad B_{L,R} \equiv \int_{-1}^0 \frac{d\sigma_{L,R}}{dz} dz. \quad (\text{B.16})$$

One can also define the final state polarization left-right asymmetry:

$$\begin{aligned} P_f^{LR} &\equiv \frac{\sigma_L^{fR} - \sigma_L^{fL} - \sigma_R^{fR} + \sigma_R^{fL}}{\sigma_L^{fR} + \sigma_L^{fL} + \sigma_R^{fR} + \sigma_R^{fL}} = -\mathcal{P}_{eff} \frac{G_-^e(1+z^2) + 2G_+^e z}{G_+^e(1+z^2) + 2G_-^e z} \\ &\rightarrow -\mathcal{P}_{eff} \frac{A_e A_f(1+z^2) + 2z}{(1+z^2) + 2A_e A_f z} \rightarrow -\mathcal{P}_{eff} A_e A_f. \end{aligned} \quad (\text{B.17})$$

References

- [1] P. Langacker, *The Physics of Heavy Z' Gauge Bosons*, *Rev.Mod.Phys.* **81** (2009) 1199–1228, [[arXiv:0801.1345](#)].
- [2] M. Cvetič and S. Godfrey, *Discovery and identification of extra gauge bosons*, [hep-ph/9504216](#).
- [3] J. L. Hewett and T. G. Rizzo, *Low-Energy Phenomenology of Superstring Inspired $E(6)$ Models*, *Phys.Rept.* **183** (1989) 193.
- [4] A. Leike, *The Phenomenology of extra neutral gauge bosons*, *Phys.Rept.* **317** (1999) 143–250, [[hep-ph/9805494](#)].
- [5] M. Cvetič and P. Langacker, *Z -prime physics and supersymmetry*, [hep-ph/9707451](#).
- [6] J. Erler, P. Langacker, S. Munir, and E. Rojas, *Improved Constraints on Z -prime Bosons from Electroweak Precision Data*, *JHEP* **0908** (2009) 017, [[arXiv:0906.2435](#)].
- [7] P. Langacker, *The Physics of New $U(1)$ -prime Gauge Bosons*, *AIP Conf.Proc.* **1200** (2010) 55–63, [[arXiv:0909.3260](#)].
- [8] P. Nath, B. D. Nelson, H. Davoudiasl, B. Dutta, D. Feldman, et al., *The Hunt for New Physics at the Large Hadron Collider*, *Nucl.Phys.Proc.Suppl.* **200-202** (2010) 185–417, [[arXiv:1001.2693](#)].
- [9] J. Jaeckel and A. Ringwald, *The Low-Energy Frontier of Particle Physics*, *Ann.Rev.Nucl.Part.Sci.* **60** (2010) 405–437, [[arXiv:1002.0329](#)].

- [10] F. del Aguila, J. de Blas, and M. Perez-Victoria, *Electroweak Limits on General New Vector Bosons*, *JHEP* **1009** (2010) 033, [[arXiv:1005.3998](#)].
- [11] R. Diener, S. Godfrey, and I. Turan, *Constraining Extra Neutral Gauge Bosons with Atomic Parity Violation Measurements*, *Phys.Rev.* **D86** (2012) 115017, [[arXiv:1111.4566](#)].
- [12] J. Kang and P. Langacker, *Z' discovery limits for supersymmetric E(6) models*, *Phys.Rev.* **D71** (2005) 035014, [[hep-ph/0412190](#)].
- [13] C.-F. Chang, K. Cheung, and T.-C. Yuan, *Supersymmetric Decays of the Z' Boson*, *JHEP* **1109** (2011) 058, [[arXiv:1107.1133](#)].
- [14] R. Robinett and J. L. Rosner, *Mass Scales In Grand Unified Theories*, *Phys.Rev.* **D26** (1982) 2396.
- [15] P. Langacker, R. W. Robinett, and J. L. Rosner, *New Heavy Gauge Bosons in p p and p anti-p Collisions*, *Phys.Rev.* **D30** (1984) 1470.
- [16] A. Czarnecki, M. Jezabek, and J. H. Kuhn, *Lepton Spectra From Decays Of Polarized Top Quarks*, *Nucl.Phys.* **B351** (1991) 70–80.
- [17] F. del Aguila, M. Cvetič, and P. Langacker, *Determination of Z-prime gauge couplings to quarks and leptons at future hadron colliders*, *Phys.Rev.* **D48** (1993) 969–973, [[hep-ph/9303299](#)].
- [18] F. Del Aguila and M. Cvetič, *Diagnostic power of future colliders for Z-prime couplings to quarks and leptons: e+ e- versus p p colliders*, *Phys.Rev.* **D50** (1994) 3158–3166, [[hep-ph/9312329](#)].
- [19] F. Del Aguila, M. Cvetič, and P. Langacker, *Reconstruction of the extended gauge structure from Z-prime observables at future colliders*, *Phys.Rev.* **D52** (1995) 37–43, [[hep-ph/9501390](#)].
- [20] M. Dittmar, A.-S. Nicollerat, and A. Djouadi, *Z-prime studies at the LHC: An Update*, *Phys.Lett.* **B583** (2004) 111–120, [[hep-ph/0307020](#)].
- [21] M. S. Carena, A. Daleo, B. A. Dobrescu, and T. M. Tait, *Z' gauge bosons at the Tevatron*, *Phys.Rev.* **D70** (2004) 093009, [[hep-ph/0408098](#)].
- [22] **LHC/LC Study Group** Collaboration, G. Weiglein et al., *Physics interplay of the LHC and the ILC*, *Phys.Rept.* **426** (2006) 47–358, [[hep-ph/0410364](#)].
- [23] F. Petriello and S. Quackenbush, *Measuring Z' couplings at the CERN LHC*, *Phys.Rev.* **D77** (2008) 115004, [[arXiv:0801.4389](#)].
- [24] S. Godfrey and T. A. Martin, *Identification of Extra Neutral Gauge Bosons at the LHC Using b- and t-Quarks*, *Phys.Rev.Lett.* **101** (2008) 151803, [[arXiv:0807.1080](#)].
- [25] P. Osland, A. Pankov, A. Tsytrinov, and N. Paver, *Spin and model identification of Z' bosons at the LHC*, *Phys.Rev.* **D79** (2009) 115021, [[arXiv:0904.4857](#)].
- [26] Y. Li, F. Petriello, and S. Quackenbush, *Reconstructing a Z-prime Lagrangian using the LHC and low-energy data*, *Phys.Rev.* **D80** (2009) 055018, [[arXiv:0906.4132](#)].
- [27] R. Diener, S. Godfrey, and T. A. Martin, *Discovery and Identification of Extra Neutral Gauge Bosons at the LHC*, [[arXiv:0910.1334](#)].
- [28] R. Diener, S. Godfrey, and T. A. Martin, *Unravelling an Extra Neutral Gauge Boson at the LHC using Third Generation Fermions*, *Phys.Rev.* **D83** (2011) 115008, [[arXiv:1006.2845](#)].

- [29] S. Gopalakrishna, T. Han, I. Lewis, Z.-g. Si, and Y.-F. Zhou, *Chiral Couplings of W' and Top Quark Polarization at the LHC*, *Phys.Rev.* **D82** (2010) 115020, [[arXiv:1008.3508](#)].
- [30] J. Erler, P. Langacker, S. Munir, and E. Rojas, *Z' Bosons at Colliders: a Bayesian Viewpoint*, *JHEP* **1111** (2011) 076, [[arXiv:1103.2659](#)].
- [31] E. L. Berger, Q.-H. Cao, C.-R. Chen, and H. Zhang, *Top Quark Polarization As A Probe of Models with Extra Gauge Bosons*, *Phys.Rev.* **D83** (2011) 114026, [[arXiv:1103.3274](#)].
- [32] C.-W. Chiang, N. D. Christensen, G.-J. Ding, and T. Han, *Discovery in Drell-Yan Processes at the LHC*, *Phys.Rev.* **D85** (2012) 015023, [[arXiv:1107.5830](#)].
- [33] E. Accomando, D. Becciolini, A. Belyaev, S. Moretti, and C. Shepherd-Themistocleous, *Z' at the LHC: Interference and Finite Width Effects in Drell-Yan*, [[arXiv:1304.6700](#)].
- [34] E. L. Berger, Q.-H. Cao, J.-H. Yu, and H. Zhang, *Measuring Top-Quark Polarization in Top-Pair + Missing Energy Events*, [[arXiv:1305.7266](#)].
- [35] **ATLAS** Collaboration, ATLAS-CONF-2013-017, *Search for high-mass dilepton resonances in 20/fb of pp collisions at $\sqrt{s} = 8$ TeV with the ATLAS experiment*, .
- [36] **CMS** Collaboration, EXO12061, *Search for Resonances in the Dilepton Mass Distribution*, .
- [37] J. Alwall, M. Herquet, F. Maltoni, O. Mattelaer, and T. Stelzer, *MadGraph 5 : Going Beyond*, *JHEP* **1106** (2011) 128, [[arXiv:1106.0522](#)].
- [38] N. D. Christensen and C. Duhr, *FeynRules - Feynman rules made easy*, *Comput.Phys.Commun.* **180** (2009) 1614–1641, [[arXiv:0806.4194](#)].
- [39] J. Pumplin, D. Stump, J. Huston, H. Lai, P. M. Nadolsky, et al., *New generation of parton distributions with uncertainties from global QCD analysis*, *JHEP* **0207** (2002) 012, [[hep-ph/0201195](#)].
- [40] T. Sjostrand, S. Mrenna, and P. Z. Skands, *PYTHIA 6.4 Physics and Manual*, *JHEP* **0605** (2006) 026, [[hep-ph/0603175](#)].
- [41] S. Ovin, X. Rouby, and V. Lemaitre, *DELPHES, a framework for fast simulation of a generic collider experiment*, [[arXiv:0903.2225](#)].
- [42] **ECFA/DESY LC Physics Working Group** Collaboration, E. Accomando et al., *Physics with e^+e^- linear colliders*, *Phys.Rept.* **299** (1998) 1–78, [[hep-ph/9705442](#)].
- [43] S. Godfrey, P. Kalyniak, and A. Tomkins, *Distinguishing between models with extra gauge bosons at the ILC*, [[hep-ph/0511335](#)].
- [44] P. Osland, A. Pankov, and A. Tsytrinov, *Identification of extra neutral gauge bosons at the International Linear Collider*, *Eur.Phys.J.* **C67** (2010) 191–204, [[arXiv:0912.2806](#)].
- [45] L. Linssen, A. Miyamoto, M. Stanitzki, and H. Weerts, *Physics and Detectors at CLIC: CLIC Conceptual Design Report*, [[arXiv:1202.5940](#)].
- [46] H. Baer et al., *Physics at the International Linear Collider, Technical Design Report*, .
- [47] M. Battaglia, F. Coradeschi, S. De Curtis, and D. Dominici, *Indirect Sensitivity to Heavy Z' Bosons at a Multi-TeV $e+e-$ Collider*, [[arXiv:1203.0416](#)].
- [48] T. Behnke, J. E. Brau, P. N. Burrows, J. Fuster, M. Peskin, et al., *The International Linear Collider Technical Design Report - Volume 4: Detectors*, [[arXiv:1306.6329](#)].
- [49] H. Baer, T. Barklow, K. Fujii, Y. Gao, A. Hoang, et al., *The International Linear Collider Technical Design Report - Volume 2: Physics*, [[arXiv:1306.6352](#)].

- [50] A. Freitas, K. Hagiwara, S. Heinemeyer, P. Langacker, K. Moenig, et al., *Exploring Quantum Physics at the ILC*, [arXiv:1307.3962](https://arxiv.org/abs/1307.3962).
- [51] A. Blondel, *A Scheme To Measure The Polarization Asymmetry At The Z Pole In LEP*, *Phys.Lett.* **B202** (1988) 145.